AD-A172 762 APPLICABILITY OF THE LIQUID CRYSTAL TELEVISION FOR 1/1
OPTICAL DATA PROCESSING(U) JET PROPULSION LAB PASADENA
CA J A DAVIS ET AL 1986 ARO-22329 2-PH
UNCLASSIFIED N00014-85-K-0599 F/G 17/2 NL

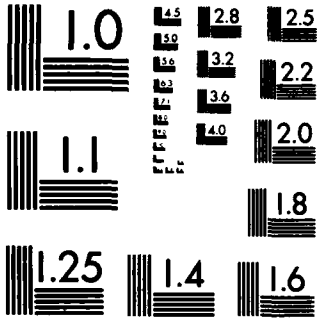

UNCLASSI
SECURITY CLAS

AD-A172 762 DOCUMENTATION PAGE

1a. REPORT SEC Unclassified	1b. RESTRICTIVE MARKINGS
2a. SECURITY CLASSIFICATION AUTHORITY	3. DISTRIBUTION/AVAILABILITY OF REPORT Approved for public release; distribution unlimited.
2b. DECLASSIFICATION/DOWNGRADING SCHEDULE	
4. PERFORMING ORGANIZATION REPORT NUMBER(S)	5. MONITORING ORGANIZATION REPORT NUMBER(S) ARO 22329.2-PH
6a. NAME OF PERFORMING ORGANIZATION Jet Propulsion Lab. California Inst. of Technology 6b. OFFICE SYMBOL (If applicable)	7a. NAME OF MONITORING ORGANIZATION U. S. Army Research Office
6c. ADDRESS (City, State, and ZIP Code) Pasadena, CA 91109	7b. ADDRESS (City, State, and ZIP Code) P. O. Box 12211 Research Triangle Park, NC 27709-2211
8a. NAME OF FUNDING/SPONSORING ORGANIZATION U. S. Army Research Office 8b. OFFICE SYMBOL (If applicable)	9. PROCUREMENT INSTRUMENT IDENTIFICATION NUMBER MIPR ARO 133-86
8c. ADDRESS (City, State, and ZIP Code) P. O. Box 12211 Research Triangle Park, NC 27709-2211	10. SOURCE OF FUNDING NUMBERS PROGRAM ELEMENT NO. / PROJECT NO. / TASK NO. / WORK UNIT ACCESSION NO.

11. TITLE (Include Security Classification)
Applicability of the Liquid Crystal Television for Optical Data Processing

12. PERSONAL AUTHOR(S)
Jeffrey A. Davis, Roger A. Lilly, Kevin D. Krenz, Hua-Kuang Liu

13a. TYPE OF REPORT	13b. TIME COVERED	14. DATE OF REPORT (Year, Month, Day)	15. PAGE COUNT
Reprint	FROM _____ TO _____		

16. SUPPLEMENTARY NOTATION
The view, opinions and/or findings contained in this report are those of the author(s) and should not be construed as an official Department of the Army position, policy, or decision, unless so designated by other documentation.

17. COSATI CODES		
FIELD	GROUP	SUB-GROUP

18. SUBJECT TERMS (Continue on reverse if necessary and identify by block number)

19. ABSTRACT (Continue on reverse if necessary and identify by block number)

ABSTRACT ON REPRINT

DTIC FILE COPY

DTIC ELECTE OCT 10 1986 D

20. DISTRIBUTION/AVAILABILITY OF ABSTRACT ☐ UNCLASSIFIED/UNLIMITED ☐ SAME AS RPT. ☐ DTIC USERS	21. ABSTRACT SECURITY CLASSIFICATION Unclassified
22a. NAME OF RESPONSIBLE INDIVIDUAL	22b. TELEPHONE (Include Area Code) / 22c. OFFICE SYMBOL

DD FORM 1473, 84 MAR 83 APR edition may be used until exhausted. All other editions are obsolete.

SECURITY CLASSIFICATION OF THIS PAGE
UNCLASSIFIED

DISCLAIMER NOTICE

THIS DOCUMENT IS BEST QUALITY PRACTICABLE. THE COPY FURNISHED TO DTIC CONTAINED A SIGNIFICANT NUMBER OF PAGES WHICH DO NOT REPRODUCE LEGIBLY.

Applicability of the liquid crystal television for optical data processing

Jeffrey A. Davis, Roger A. Lilly, and Kevin D. Krenz

Department of Physics, San Diego State University
San Diego, California 92182

Hua-Kuang Liu

Jet Propulsion Laboratory, California Institute of Technology
Pasadena, California 91109

Abstract

The pocket-size liquid crystal television (LCTV) has been investigated for its potential as a two dimensional spatial light modulator. The LCTV can be addressed using both a microcomputer and a TV camera. We have measured various characteristics of this device including transmission control, bipolar modulation capabilities, and have tested its usage as an input device for an optical correlator. Optical phase distortions of the device can be compensated by a liquid gate. These results suggest that this device has great potential for optical pattern recognition and optical data processing applications.

Introduction

Optical data processing and optical pattern recognition are mainly limited by the capability and availability of real-time two-dimensional spatial light modulators (SLM's). Among the many types of SLM's which have been developed are the liquid crystal light valve (LCLV)[1,3], the magneto-optic spatial light modulator[2], the microchannel spatial light modulator[4], the Pockels readout optical modulator[5], and the deformable mirror device[5]. However, these SLM's are very expensive or are still in R & D stages. Recently however, several versions of a small inexpensive compact liquid crystal television (LCTV) have become commercially available. We have investigated the properties of one of these for optical data processing applications.

The Radio Shack LCTV (Realistic Pocketvision Cat. No. 16-151 or 16-153) has a 5.4 cm by 4.4 cm screen. The unit consists of a two-dimensional grid of raster-scanned liquid crystal cells, each of which is capable of modulating coherent or incoherent light transmitted through it. The LCTV which we investigated has a resolution of 146 horizontal elements by 120 vertical elements. Each unit cell is 370 μm x 370 μm square. The LCTV comes equipped with a video input jack which allows an image to be written electronically with a microcomputer or with a TV camera.

Experimental Results

For most of our experiments, we used the computer input mode. Using an Apple II microcomputer, the high resolution screen with 280 horizontal by 192 vertical pixels addresses 111 horizontal by 96 vertical cells on the LCTV screen. Therefore, there is a 2/1 match of vertical elements allowing exact registration. However, the horizontal registration is inexact causing edge blurring.

A commercial television camera was also used to provide an input scene and gray scale operation was verified by changing the F-stop on the camera.

Each cell of the LCTV screen is a 90° twisted nematic liquid crystal sandwiched between parallel polarizers. When no electric field is applied, the plane of polarization for linearly polarized light incident on the cell is rotated through 90° by the twisted liquid crystal molecules and no light is transmitted through the second polarizer. However, under an applied electric field, the twist and tilt of the liquid crystal molecules are altered affecting the rotation angle of the transmitted light and therefore varying the amount of light transmitted through the second polarizer.

Voltage is applied to each pixel through horizontal and vertical line electrodes which intersect at each pixel. The voltage applied to each pixel is determined by two factors. First, an adjustable BRIGHTNESS control adjusts a uniform voltage onto every pixel which allows the transmission level of the entire screen to be uniformly varied. In addition, the input signal from the TV receiver, the computer, or the TV camera then varies the individual voltage applied to each pixel, thus modulating the individual transmission of each pixel and creating the picture.

Experiments studying the polarization of the light transmitted by the liquid crystal cells were performed after the second polarizer was removed from the LCTV. The transmitted polarization state was analyzed with a second rotatable polarizer as a function of bias voltage across the LCTV at the He-Ne laser wavelength of 632.8 nm. Control of this voltage was provided by the brightness adjustment. In order to obtain an arbitrary yet quantitative measurement of this voltage, we took the LCTV apart and measured the voltage drop across the variable resistor which controls the brightness. This resistor is designated RV801 on the circuit schematic given in the REALISTIC service manual. The laser beam was expanded to cover a large number of pixels.

These experiments showed that the plane of polarization transmitted through the liquid crystal elements was essentially linear and rotated as the brightness control voltage was varied as shown in Figure 1. The two curves show the results when the computer monitor was addressing every pixel (termed the On state) and when the computer monitor was turned off. The two curves essentially differ by a rotation angle of 11°. Note that the initial rotation angle with no applied voltage (corresponding to -1.7 V) was only 73° and not the expected 90°. We feel that this indicates that the initial polarizer was not accurately aligned with the direction of the liquid crystal molecules. The output polarization was essentially linear with a slight orthogonal component which is also probably due to this misalignment. Therefore, the device operates very similarly to the LCLV and the magneto-optic SLM. The transmitted light intensity will then vary as the computer voltage is changed. However, the exact nature of the transmitted light will depend on the angle of the second polarizer as well as the brightness control voltage.

Previous investigations of the LCTV[6] have shown that there is a phase nonuniformity across the surface which destroys much of its capability as a SLM. This was examined next by studying the Fraunhofer diffraction pattern produced by the device. Light from the He-Ne laser was collimated and sent through a 36.8 cm focal length lens. A diode array detector placed in the focal plane of the lens was used to record the Fraunhofer diffraction pattern. Figure 2A shows the focused spot produced by the system. Figure 2B shows the broadening of the focused spot when the LCTV was introduced into the system. This broadening is evidence of phase nonuniformity across the plane of the LCTV.

These phase variations were correctable by placing the LCTV inside a Newport Corporation model 550-G liquid gate filled with mineral oil. This successfully eliminated the phase variations as shown by the sharpened focused spot in Figure 2C. The liquid gate is used in the remainder of these experiments.

We next explored the use of this device as a bipolar modulator which has previously been demonstrated for the Litton magneto-optic SLM[7]. As discussed earlier, light transmitted by the LCTV has two polarization states which are rotated by a maximum of 11° to each other depending on the state of each pixel. The transmitted light intensity then depends on the orientation of the second polarizer. Results of varying the angle of this second polarizer were examined in the Fraunhofer diffraction of a pattern placed on the LCTV.

A grid pattern was written with every other horizontal line of the LCTV addressed by the microcomputer. Recall the exact registration between the computer output and the TV screen which allows this. The orientation of the second polarizer was adjusted to completely block the transmitted light from the pixels which were not addressed resulting in the transmission pattern as shown in Figure 3A. The Fraunhofer diffraction pattern will consist of a high DC peak with first order peaks whose intensities are $4/\pi^2$ smaller than the DC peak as shown in Figure 3B.

Bipolar operation of the LCTV can be achieved by orienting the second linear polarizer perpendicular to the bisector of the two transmitted polarization states as shown in Figure 4A. Therefore the electric field passed by the pixels will only differ by a phase term of π radians resulting in the electric field amplitude transmission pattern of Figure 4B. The Fraunhofer diffraction pattern for this will have no DC component. The orientation of the analyzer was adjusted to achieve the transmission pattern of Figure 4B and results are shown in Figure 4C. We see a dramatic reduction in the size of the DC peak relative to Figure 3B. Although the size of the DC term is greatly reduced, there is still some DC transmission. There are several possible explanations for this. First, we observe that the pattern on the LCTV is not uniform possibly due to a voltage nonuniformity across the face of the screen. Second, there are areas between the individual pixels which are not affected by the applied voltage. Finally, each pixel is sequentially addressed and there is a time lag between the addressing of each pixel during which the orientation of the liquid crystal molecules can relax to their original positions. Therefore the transmission state of each pixel will vary slightly with time contributing to a DC term. Nevertheless, this capability for bipolar modulation is identical to that recently reported for the magneto-optic SLM[7].

A series of measuremgnts were then made using the LCTV as the input screen for a Vander Lugt optical correlator[8]. The correlation system geometry is shown in Figure 5. Collimated

A-1

light from a spatially filtered beam is incident on plane P1 where the input pattern is placed using the LCTV. The Fourier transform plane P2 is obtained using a 75 cm focal length lens. The reference beam was also spatially filtered and collimated and then focused using a long focal lens to plane P3 located beyond plane P2. This converging reference beam is used to eliminate the final Fourier transform lens [9,10]. Matched spatial filters (MSF) were then recorded using a Newport Corporation model HC-300 thermoplastic recording camera. The focused reference beam synthesizes a Fresnel zone plate within the MSF. Care was taken in recording the MSF to emphasize the spatial frequencies corresponding to the grating information shown in Figure 4B and not the grid information. The MSF was made using the grid pattern with every other horizontal line of the LCTV turned on as before.

Plane P3 contains the correlation between the input pattern and the pattern used in recording the MSF and is shown in Figure 6. This correlation spike is much sharper than previously reported[6], again due to the liquid gate. Note also the sideband spikes corresponding to the correlation of the pattern with a shifted version of itself. The size of the correlation spike decreased as before[6] as the period of the input pattern varied both above and below the period used in making the MSF. As before, the correlation spike disappeared when the LCTV was made uniformly transparent of the LCTV elements, then the spike would have been still evident.

Preliminary experiments using the TV camera to address the LCTV have shown translation invariance of the correlation spike and will be reported in more detail in the future.

Conclusions

In conclusion, our experiments show that the LCTV can be used as a highly versatile SLM. It most closely matches the operational characteristics of the Litton magneto-optic SLM in terms of resolution and operation including the capability for bipolar modulation. Although phase nonuniformity is still a problem, it appears that it can be corrected using the liquid gate. Moreover, it is very inexpensive, is easily connected to computers, and satisfies many of the prerequisites for SLM's. Finally, it will allow many experimentalists to enter the field of optical pattern recognition at substantially reduced expenses and may prove to be an impetus to an explosion of activity in this field.

This research is partially supported by NASA and partially by the Physics Division of the Army Research Office through contract with the Jet Propulsion Laboratory. We wish to acknowledge the expert technical assistance of *M. Hatay of S.D.S.U.*

References

1. J. Grinberg, A. Jacobsen, W. Bleha, L. Miller, L. Fraas, D. Boswell, and G. Meyer, Opt. Eng., 14, 217, (1975)
2. W.E. Ross, D. Psaltis, and R.H. Anderson, Opt. Eng., 22, 485, (1983)
3. C. Warde, A.M. Weiss, A.D. Fisher, and J.I. Thackara, Appl. Opt., 20, 2066, (1981)
4. R. Sprague, J. Appl. Phys., 46, 1673, (1975)
5. L.J. Hornbeck, IEEE Trans. Electron Devices, ED-30, 539, (1983)
6. H.K. Liu, J.A. Davis, and R.A. Lilly, Opt. Letters, 10, 635, (1985)
7. D. Psaltis, E.G. Paek, and S.S. Venkatesh, Opt. Eng., 23, 698, (1984)
8. A. Vander Lugt, IEEE Trans. Inf. Theory, IT-10, 139, (1964)
9. W. Maloney, Appl. Opt., 10, 2127, (1971)
10. M. Bage and M. Beddoes, Appl. Opt., 15, 2830, (1976)

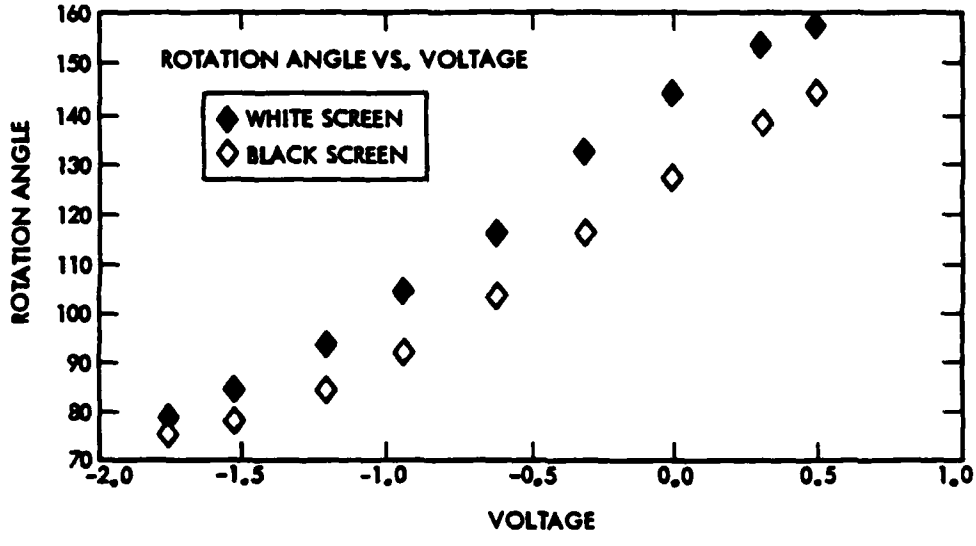

Figure 1. Rotation angle of light transmitted by LCTV cells versus brightness control voltage. Curves show data for screen when computer addresses each pixel (dark triangles), and when computer turns each pixel off (open triangles).

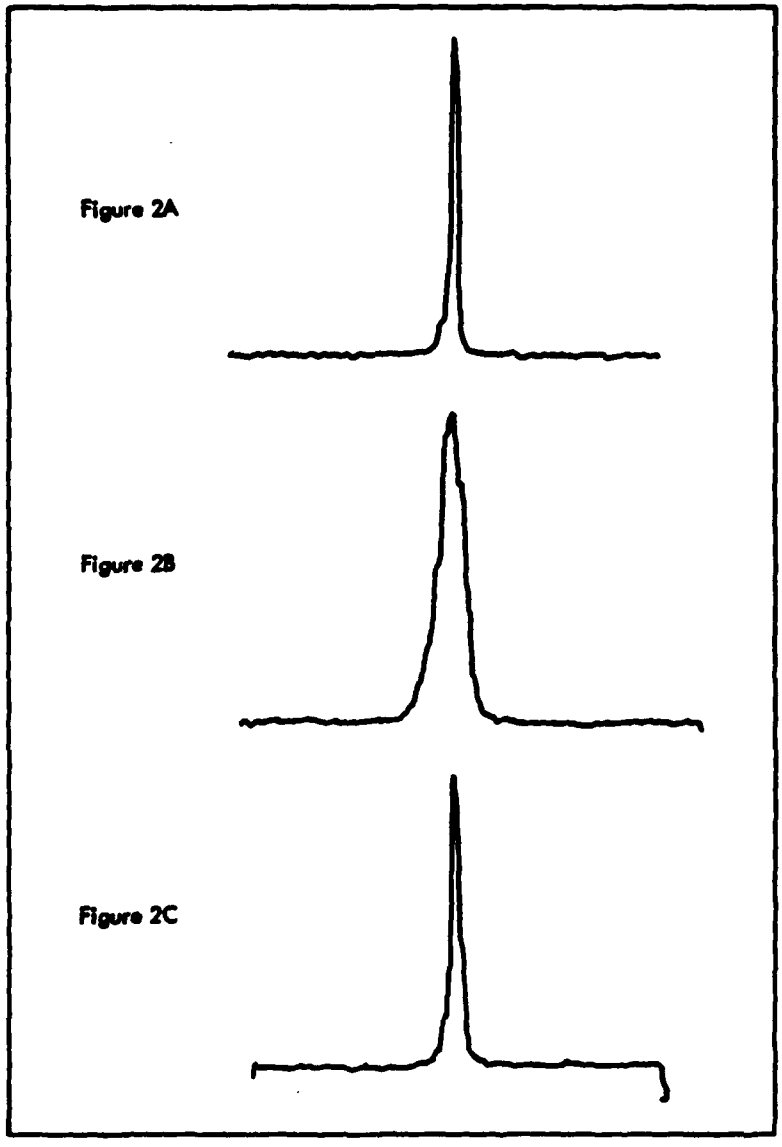

Figure 2. Fraunhofer diffraction pattern of collimated beam using 36.8 cm focal length lens and diode array detector;
A. With nothing placed in optical path
B. With LCTV placed in optical path
C. With LCTV and liquid gate placed in optical path
Note full horizontal scale is 1.6 mm.

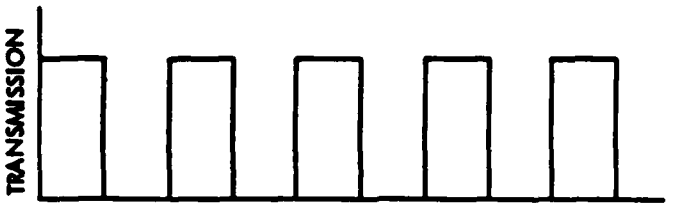

Figure 3A. Transmission versus position for on-off grid pattern.

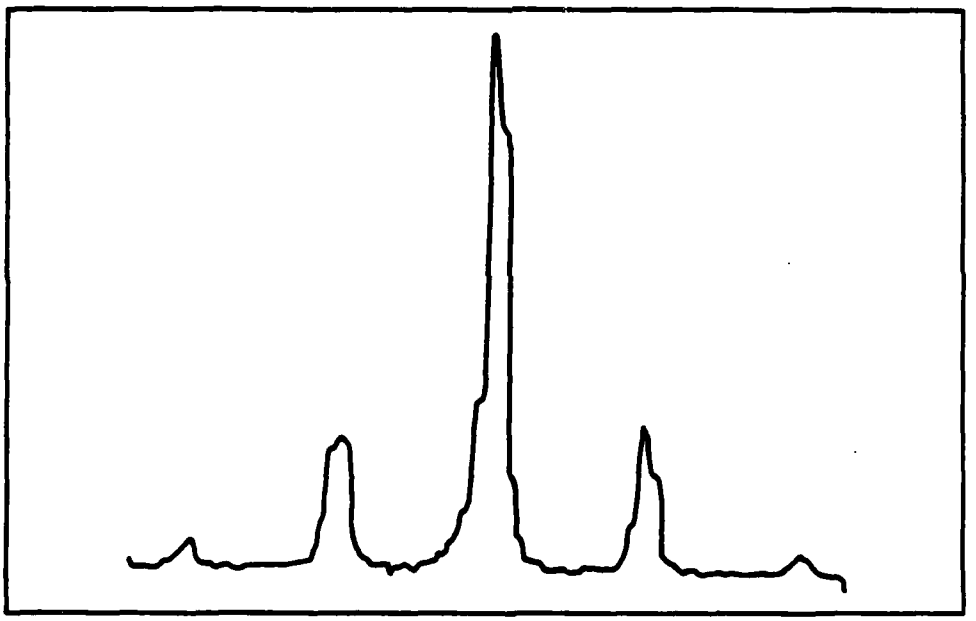

Figure 3B. Fraunhofer diffraction pattern for on-off grid in Figure 3B. Horizontal scale is 1.6 mm.

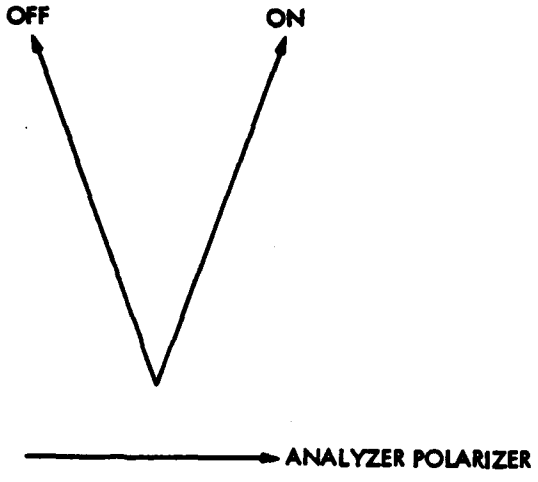

Figure 4A. Orientation of analyzer polarizer to achieve bipolar modulation.

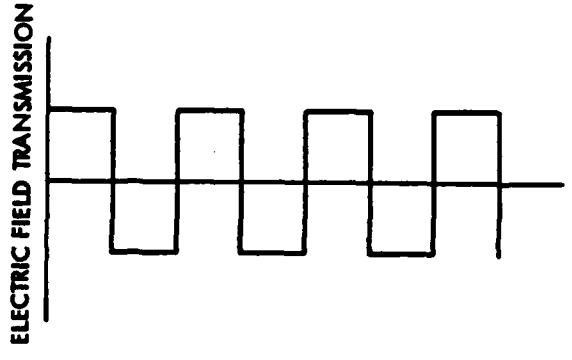

Figure 4B. Transmission versus position for bipolar modulation grid pattern.

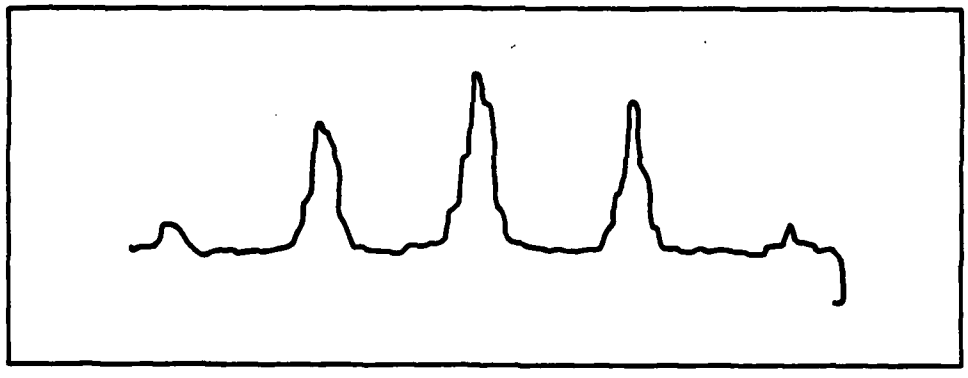

Figure 4C. Fraunhofer diffraction pattern for bipolar grid pattern in Figure 4B. Horizontal scale is 1.6 mm.

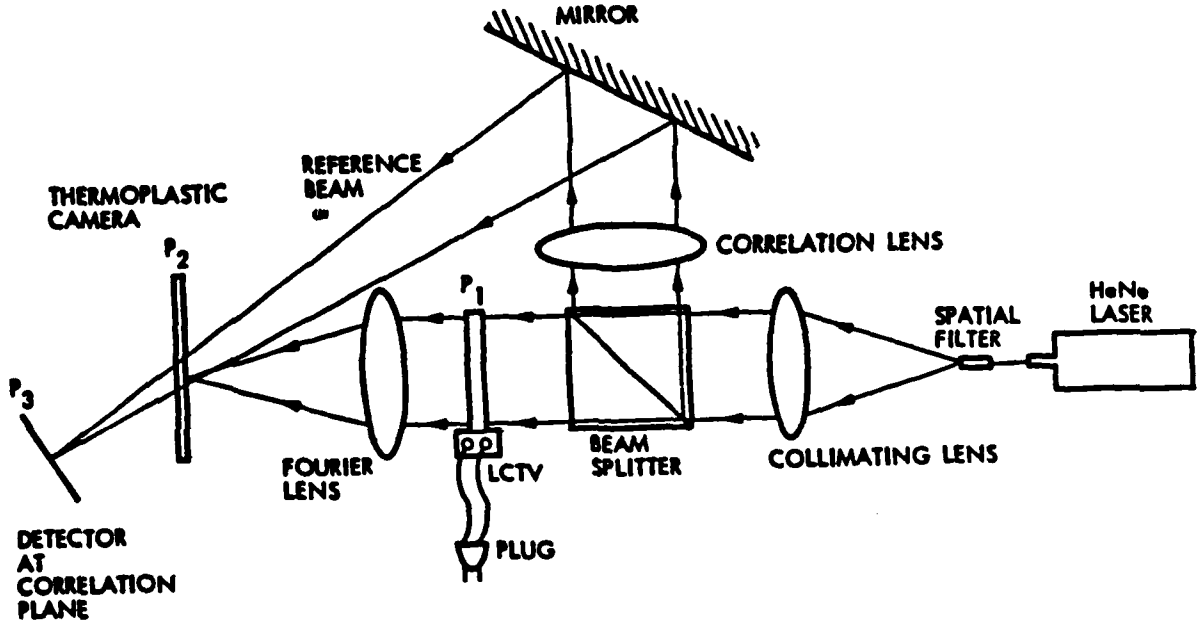

Figure 5. Optical correlator geometry used in making matched spatial filters and observing correlation signals.

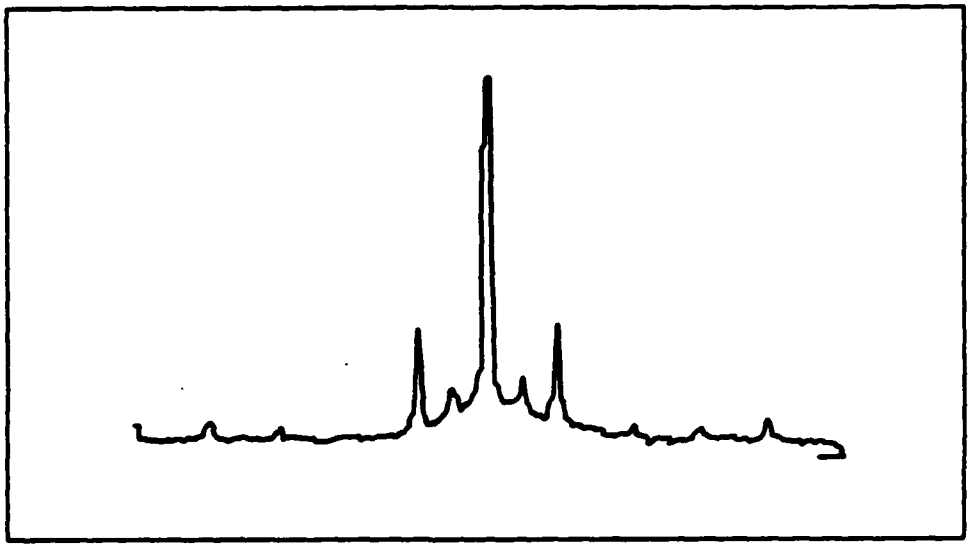

Figure 6. Cross correlation pattern due to MSF of ruling pattern on LCTV screen addressed by identical LCTV pattern.

Optical-data-processing properties of a liquid-crystal television spatial light modulator

Hua-Kuang Liu
Jeffrey A. Davis and Roger A. Lilly

a reprint from Optics Letters
volume 10, number 12, December, 1985

Optical-data-processing properties of a liquid-crystal television spatial light modulator

Hua-Kuang Liu

Jet Propulsion Laboratory, California Institute of Technology, Pasadena, California 91109

Jeffrey A. Davis and Roger A. Lilly

Department of Physics, San Diego State University, San Diego, California 92182

Received July 10, 1985; accepted September 12, 1985

The potential of the extremely inexpensive Radio Shack liquid-crystal television (LCTV) as a two-dimensional spatial light modulator has been investigated. The LCTV modulates the transmission of coherent or incoherent light and can either be electronically addressed through a microcomputer or optically addressed with a TV camera. We have measured the transmission characteristics of the device, examined its diffraction pattern, and tested its use as an input device for an optical correlator. We have discovered that, with proper modifications, it has potential for optical-data-processing applications.

It is well known that optical data processing and optical computing are limited mainly by the capability and availability of real-time devices, such as two-dimensional spatial light modulators (SLM's). For this reason, great efforts by many researchers have been spent in search for usable SLM's. Existing and developing SLM's include the liquid-crystal light valve,[1] the magneto-optic spatial light modulator,[2] the microchannel spatial light modulator,[3] the Pockels readout optical modulator,[4] and the deformable mirror device.[5]

Many SLM's are either forbiddingly expensive or are still in R&D stages. Recently, several small inexpensive compact liquid-crystal televisions (LCTV's) became commercially available. We have investigated the properties of the Radio Shack LCTV for optical-data-processing applications, and what follows is a brief account of our discoveries.

The LCTV has a 5.4-cm by 4.4-cm screen. The unit consists of a two-dimensional mosaic of raster-scanned liquid-crystal cells, each of which is capable of modulating the coherent or incoherent light transmitted through it. The resolution of the LCTV is determined by the number of cells in the screen. The LCTV under investigation has 146 horizontal elements by 120 vertical elements. Each unit cell is 370 μm × 370 μm square. The LCTV is equipped with a video input jack, which allows an image to be written electronically with a microcomputer or optically with a TV camera.

For most of our experiments, we have used the computer input mode. When an Apple II+ microcomputer is used, the high-resolution screen with 280 horizontal × 192 vertical pixels addresses 111 horizontal × 96 vertical elements of the LCTV. Therefore, there is a 2 to 1 match of vertical elements, permitting exact registration. However, the horizontal registration is off, causing edge blurring.

A TV camera was also used to provide an input scene, and gray-scale operation was verified by changing the *f*-stop on the camera.

Each liquid-crystal cell of the TV screen is a 90° twisted nematic liquid crystal sandwiched between parallel polarizers. When no electric field is applied, the plane of polarization for linearly polarized light is rotated through 90° by the twisted liquid-crystal molecules, and no light is transmitted through the second polarizer.

However, under an applied electric field, the twist and the tilt of the liquid-crystal molecules are altered, resulting in a greater fraction of the light retaining the initial polarization direction. As the electric field is increased further, the molecules do not affect the plane of polarization, and all the light passes through the second polarizer. Transmission losses are then limited to the transmission of two polarizer sheets.

Voltage is applied to each pixel through horizontal and vertical line electrodes, which intersect at each pixel. The voltage applied to each pixel is determined by two factors. First, a brightness control determines a bias voltage across every cell that allows the transmission level of the entire screen to be varied. The input signal from the TV receiver, the computer, or the TV camera then varies the individual voltage applied to each cell modulating the individual transmission of each cell, thus creating a SLM with gray-scale capability.

We have performed a series of experiments on the LCTV. Measurements have been made of the optical transmission at the He–Ne laser wavelength as a function of bias voltage across the liquid-crystal unit cells. Control of this voltage is provided by the brightness adjustment on the LCTV. In order to obtain a quantitative measurement, we took the LCTV apart and measured the voltage drop across the variable resistor controlled by the brightness control. (The voltage across a cell is not directly accessible.) The laser

0146-9592/85/120635-03$2.00/0

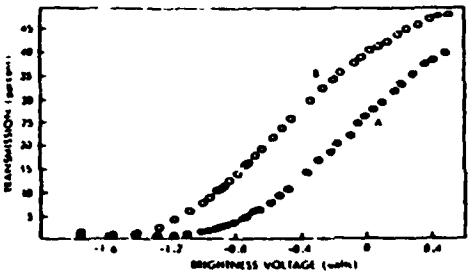

Fig. 1. Transmission measurements of the LCTV as a function of bias voltage. Curve A shows results with the computer pixels turned off; curve B shows results with the computer pixels turned on.

beam was expanded to cover a 1-cm^2 area of the LCTV screen to average over a large number of pixels. The percentage transmission versus voltage is shown as curve A of Fig. 1. The maximum transmission obtainable is 50%, and the full contrast is about 25/1.

Next, the transmission was measured as the computer wrote uniformly on the LCTV. The computer output places an additional voltage on each cell, modulating its transmission with results shown as curve B of Fig. 1. The computer voltage has the effect of shifting curve A by about −0.4 V. Therefore the operation of the LCTV using a computer input consists of picking a bias point, using the brightness control, and then having the computer change the bias voltage and the resulting transmission at any pixel.

Maximum contrast is obtained by biasing the brightness control at −0.4 V. The high slope of the transmission-versus-voltage curve ensures that the computer will cause a maximum change in transmission. In many SLM applications, it is important to turn all unused unit cells off, and the preferred bias point is at −1.2 V. However, when the pixels are turned on, the transmission increases only to 5%, with the contrast significantly decreased. This change in the voltage applied to each unit cell is set by the TV circuitry. Attempts to increase this voltage swing for higher contrast were unsuccessful. These included varying the video gain and the analog-to-digital converter adjustment inside the TV and externally amplifying the rf signal from the computer. Therefore, without extensive modification, computer operation of the LCTV can provide only minimal binary transmission.

Measurements also have been made of the Fraunhofer diffraction pattern for light incident upon the LCTV; they are shown in Fig. 2 (a). As expected from theoretical predictions, the prominent pattern is representative of the grid-matrix type of cell structure of the LCTV elements. Figure 2(b) shows the results when a horizontal grating is written on the LCTV screen with every other line turned on. The expected additional diffraction spots are clearly visible.

Finally, series of measurements have been made using the LCTV as the input screen for a Vander Lugt optical correlator.[6] The correlation system geometry is shown in Fig. 3. Collimated light from a spatially filtered beam is incident upon plane P_1, where the input pattern is placed using the LCTV. The Fourier transform plane P_2 is obtained using a 75-cm focal-length lens. The reference beam was also spatially filtered and collimated and then focused using a long-focal-length lens to plane P_3 located beyond plane P_2. This converging reference beam is used to eliminate the final Fourier-transform lens.[7,8] Matched spatial filters (MSF's) were recorded using a Newport Corporation Model HC-300 thermoplastic recording camera. The focused reference beam synthesizes a Fresnel zone plate within the MSF. Care was taken in recording the MSF to emphasize the spatial frequencies corresponding to the grating information shown in Fig. 2(b) and not the grid information shown in Fig. 2(a). The MSF was made using a computer-generated Ronchi ruling having a period of 10 pixel lines on the high-resolution computer screen.

Plane P_3 contains the correlation between the input pattern and the pattern used in the recording of the MSF. When different computer-generated Ronchi ruling patterns appeared on the LCTV, the correlation spikes were measured using a diode array; results are shown in Fig. 4. Figure 4(a) shows the output when the input Ronchi ruling pattern is identical to that used in making the MSF. The correlation spike is clearly seen. Figure 4(b) shows the results when a computer-generated Ronchi ruling pattern having a period of 24 lines was fed to the LCTV. The correlation spike is reduced, as expected.

The size of the correlation spike decreased as the period of the input ruling varied about the period used

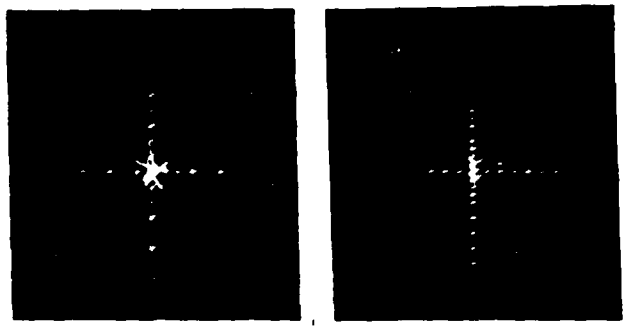

(a) (b)

Fig. 2. Fraunhofer diffraction patterns from the LCTV: (a) without (b) with a horizontal grating written onto the screen.

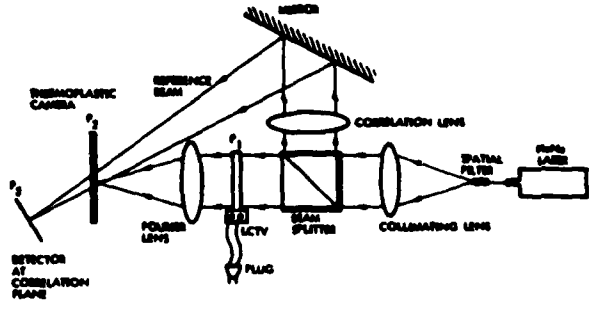

Fig. 3. Schematic of a laser MSF recording and detection system.

Fig. 4. Cross-correlation signals due to a MSF of a 10-line ruling pattern on the LCTV screen addressed by (a) 10 lines, (b) 24 lines, (c) a blank screen. The vertical axes are of the same scale with arbitrary units. The horizontal axis has a total width of 3.2 mm (=128 μm × 25 μm).

in making the MSF. Our success in optimizing the MSF is shown in Fig. 4(c), with the LCTV screen uniformly transparent where the correlation spike is almost gone. If the MSF were optimized for the spatial frequencies corresponding to the two-dimensional grid information rather than to the ruling information, the spike would still have been evident.

In conclusion, our experiments show that the LCTV can be used as a SLM. It allows data to be input easily to the LCTV screen from either a microcomputer or a TV camera. The contrast is good when the brightness control is adjusted to midrange. However, if minimum transmission is desired for various unit cells, then the maximum transmission is limited to about 5%. This transmission characteristic compares well with that of the Litton magneto-optical SLM[2] and should be improvable with changes in the internal electronic circuits of the LCTV.

At the present stage, only relatively coarse objects can be used as inputs for a real-time correlator because of limitations in the resolution and space–bandwidth product of the LCTV. Nevertheless, TV frame-rate correlation on an input image at a fixed location can be implemented. No shift invariance was observed. This is due to phase nonuniformity of the LCTV, which was discovered by us working with Psaltis's group at the California Institute of Technology campus and also pointed out by one of the reviewers of the manuscript of this Letter. However, the LCTV correlator, after further improvements and modifications, should be useful to robotic vision and space automation programs at NASA and in industry. It is also worthwhile mentioning that the low price and versatility of the LCTV SLM make it attractive for optical-image-processing pedagogical applications.

We are currently investigating other applications for this LCTV, including bipolar modulation,[9] optical subtraction,[10] high-gamma nonlinear-optical image processing, and optical division applications.[11]

The research described in this Letter was sponsored by the Physics Division of the U.S. Army Research Office and the National Aeronautics and Space Administration. The LCTV was first called to the attention of one of us (H. K. Liu) by J. G. Duthie. We thank M. Brownell and P. Dickinson for assisting in some of the measurements and M. Hatay for helping to disassemble the LCTV.

References

1. J. Grinberg, A. Jacobsen, W. Bleha, L. Miller, L. Fraas, D. Boswell, and G. Meyer, Opt. Eng. 14, 217 (1975).
2. W. E. Ross, D. Psaltis, and R. H. Anderson, Opt. Eng. 22, 485 (1983).
3. C. Warde, A. M. Weiss, A. D. Fisher, and J. I. Thackara, Appl. Opt. 20, 2066 (1981).
4. R. Sprague, J. Appl. Phys. 46, 1673 (1975).
5. L. J. Hornbeck, IEEE Trans. Electron. Devices ED-30, 539 (1983).
6. A. Vander Lugt, IEEE Trans. Inf. Theory IT-10, 139 (1964).
7. W. Maloney, Appl. Opt. 10, 2127 (1971).
8. M. Bage and M. Beddoes, Appl. Opt. 15, 2830 (1976).
9. D. Psaltis, E. G. Paek, and S. S. Venkatesh, Opt. Eng. 23, 698 (1984).
10. D. Z. Zhao and H. K. Liu, Opt. Lett. 8, 99 (1983).
11. E. Marom, B. H. Sofer, and U. Efron, Opt. Lett. 10, 43 (1985).

HIGH-GAMMA SPATIAL LIGHT MODULATOR FOR NONLINEAR OPTICAL PROCESSING

C. Warde and H. Lamela-Rivera

Department of Electrical Engineering and Computer Science
Massachusetts Institute of Technology, Cambridge, MA 02139

H. K. Liu

Jet Propulsion Laboratory
California Institute of Technology, Pasadena, CA 91109.

Abstract

This paper describes how the standard microchannel spatial light modulator can be (a) operated and (b) modified to generate a real-time, high-gamma readout characteristic. The paper also examines the use of such a device in a pulse-frequency modulation optical processor to achieve a wide range of real-time, nonlinear image and signal processing operations such as histogram measurement, density slicing, density-based artificial stereo and gray level image enhancement.

INTRODUCTION

It is well known that coding and modulation techniques are the key to the realization of a large number of two-dimensional, nonlinear image processing operations. The commonly used techniques include linear modulation of an image using Ronchi rulings[1] or sinusoidal gratings,[2] and spatial pulse-width modulation by contact screens.[3] In nonlinear processing, operations such as logarithmic transformation,[4-6] exponentation,[5,6] level slicing,[5,7] multiple isophote generation,[8,9] quantization,[10] pseudocolor,[11] A-D conversion,[5,12] subtraction,[5,13] and multiple image storage[1] can be realized. Other coding and modulation techniques include optical pulse-frequency modulation and pulse-azimuth modulation.[14] A one-dimensional optical pulse-frequency modulation technique, for example, has been used in conjunction with the variable-grating-mode liquid crystal light valve[15] to demonstrate real-time level slicing.

Unfortunately, the lack of a high-resolution, high-gamma spatial light modulator that would replace photographic film has precluded widespread use of real-time nonlinear optical processing. The microchannel spatial light modulator (MSLM)[17-21] is a device that is capable of achieving very high gamma. In this paper we describe how the standard MSLM can be (a) operated and (b) modified (Fabry-Perot MSLM) to generate a real-time, high-gamma readout characteristic. The paper also examines the use of such a device in a pulse-frequency modulation optical processor to achieve a wide range of real-time, nonlinear image and signal processing operations such as histogram measurement,[22] density slicing,[23] density-based artificial stereo,[24] and gray level image enhancement.[17]

HIGH-GAMMA CHARACTERISTIC

The desired high-gamma characteristic for nonlinear optical processing is illustrated in Fig. 1. It is a plot of log 1/T vs log E_m, and it exhibits a sharp threshold exposure, E_{th}. Here T is the modulator readout transmittance and E_m is the modulator input exposure with a threshold of E_{th}. For this negative-gamma characteristic, the readout light remains in the ON state for input exposures below threshold and is switched off for input levels above threshold. The gamma γ of the system is the slope of the linear region of this curve. That is, γ is given by

$$\gamma = \log(T_1/T_2)/\log(E_2/E_1) \qquad (1)$$

Both the standard and the Fabry-Perot MSLMs are capable of high-gamma operation, and both positive and negative gamma characteristics can be achieved. The techniques by which the gamma of an MSLM can be increased include (1) operation of the device in the nonlinear hard-clipped thresholding mode, (2) employing optical feedback around the device, and (3) converting the device to a Fabry-Perot MSLM. The Fabry Perot MSLM inherently generates a high-gamma characteristic when operated in the grid-stabilized saturation mode.

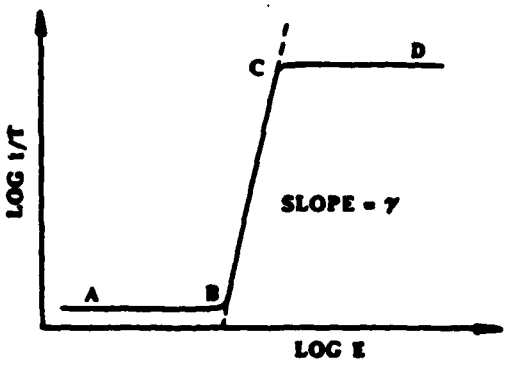

Fig. 1. Desired high-gamma characteristic.

MICROCHANNEL SPATIAL LIGHT MODULATORS

Standard MSLM

The standard Microchannel Spatial Light Modulator (MSLM)[17-21] is a versatile, real-time optical signal and image processing device that exhibits high optical sensitivity and high framing speed. It consists of a photocathode, a microchannel plate

(MCP), a planar acceleration grid and an electro-optic crystal plate, arranged in the proximity focused configuration shown in Fig. 2. The electro-optic plate carries a high resistivity dielectric mirror on one side and a transparent conducting electrode on the other.

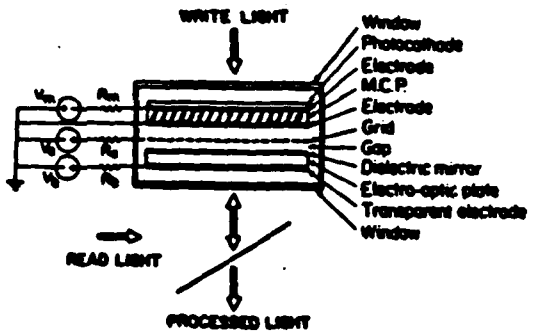

Fig. 2. The optically addressed microchannel spatial light modulator

In the electron deposition write mode, incoherent or coherent write light incident on the photocathode creates an electron image which is amplified by the MCP and proximity focused onto the dielectric mirror surface. The resulting spatially varying electric field in the crystal modulates the refractive index of the crystal. Thus, the readout light which makes a double pass through the crystal is spatially phase or amplitude modulated depending on the crystal cut and readout scheme (polarization or interferometric) employed. The image is erased by appropriately adjusting the device voltages and flooding the photocathode with light so that electrons are removed from the mirror surface by secondary electron emission.

Alternatively, the device can be operated in the reverse mode where a positive-charge image is written by secondary electron emission and erased by adding electrons to the crystal. For Pockels effect crystals, reversing the sign of the image surface charge density leads to contrast reversed images.

In the linear operating mode, the incremental surface charge density $\sigma(E)$ deposited on the crystal is proportional to the exposure E.

$$\sigma(E) = \left[\frac{\eta e G}{h\nu}\right] E \qquad (2)$$

where η is the quantum efficiency of the photocathode, e is the electronic charge, G is the gain of the MCP, h is Planck's constant and ν is the frequency of the write light. Additionally, the induced phase change $\Delta\Phi$ in the crystal is proportional to $\sigma(E)$ for Pockel's effect crystals. The exact expression depends on the type and cut of the crystal employed. For example, in oblique-cut $LiNbO_3$[18] the electrically-induced phase retardation Γ is of the form

$$\Gamma = \Phi_{y'} - \Phi_{x'} = \frac{\pi \sigma(E)}{\lambda C}\left[n_e^3 r_{y'} - n_o^3 r_{x'}\right] \qquad (3)$$

where λ is the wavelength of the exposing light, C is the capacitance per unit area of the crystal, n_o and n_e are the ordinary and extraordinary refractive indices respectively, and $r_{x'}$ and $r_{y'}$ are effective electro-optic coefficients. When such a crystal is read out between crossed polarizers, the transmittance of the crystal is given by

$$T = I_r/I_i = \sin^2(\Gamma/2) \qquad (4)$$

The most recent standard MSLMs have employed $LiNbO_3$ as the electro-optic crystal. The z-cut crystal has been used for phase modulation and an oblique cut for intensity modulation. Prototype devices employing 50-μm-thick oblique-cut $LiNbO_3$ crystals have exhibited spatial resolution of approximately 10 cycles/mm at 50% contrast.[21]

Additionally, the internal processing operations achievable with the standard MSLM include multiple-level to two-level intensity image transformation, contrast reversal, constrast enhancement, and binary level image processing operations such as, AND, NAND, OR, NOR, XOR, NXOR. However, when the standard device is operated in the linear mode its gamma is about 2, and this value is too low for nonlinear image processing applications that employ techniques such as pulse frequency modulation. Further details of the principles of operation of the standard MSLM can be found elsewhere.[17-21]

Fabry-Perot MSLM

The Fabry-Perot version of the MSLM employs a crystal that functions as an electro-optically tunable, Fabry-Perot etalon when electrons are deposited or removed from its surface. To fabricate such a crystal standard dielectric mirrors are first deposited on both surfaces of the crystal and then a transparent conducting overcoat is deposited on the readout surface of the crystal. The phase change Φ which results from the electrically induced refractive index change Δn is, to a good approximation, proportional to the surface charge density $\sigma(E)$ at the crystal surface and to the modulator write light exposure E_m [See Eqs. (2) and (3)].

For a Fabry-Perot etalon with surfaces of reflectivity R, it is well known that the ratio, T, of the total reflected intensity to the incident intensity is given by

$$T = I_r/I_i = \frac{4R\sin^2(\frac{\Phi}{2})}{(1-R)^2 + 4R\sin^2(\frac{\Phi}{2})} \qquad (5)$$

Shown in Fig. 3 is a plot of T vs Φ as given by Eq. (5). Note that the reflected readout transmittance of the MSLM approaches zero when Φ takes on integer multiples of 2π radians.

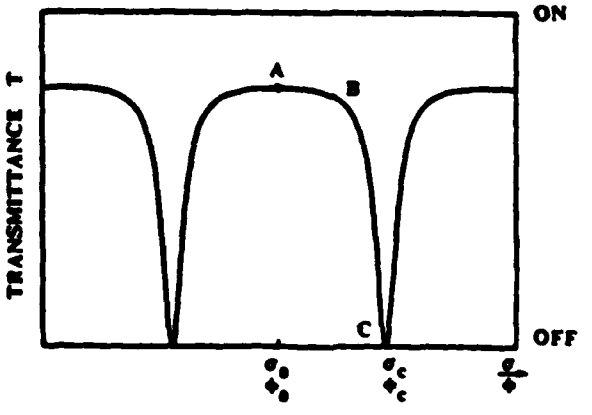

Fig. 3. Interferometric readout intensity characteristic of a Fabry-Perot crystal with R = 80 %

Fabry-Perot MSLM With Grid-Controlled Saturation

Because the region A-B-C of the Fabry-Perot characteristic (Fig. 3) closely approximates the corresponding region of the desired high-gamma characteristic (Fig. 1), the Fabry-Perot MSLM will generate the high gamma characteristic when operated in the electron deposition mode with grid stabilized saturation. The device is initially started at the point A (ON state) by precharging the crystal with a uniform surface charge density σ_o. This is accomplished by flooding the photocathode with light and setting the grid voltage to a value V_o such that the crystal surface saturates at the corresponding surface charge density σ_o. Then, by exposing the photocathode with the grid voltage set at V_c, the readout light follows the characteristic in Fig. 3 until the crystal surface voltage reaches V_c with a corresponding charge density of σ_c. Additional exposure has no effect on the readout light because of grid-limited surface charge accumulation. Thus, the high-gamma characteristic of Fig. 1 is achieved.

Hard-Clipped Thresholding Mode

Both the standard and the Fabry-Perot MSLMs can be operated in the hard-clipped thresholding mode to achieve high gamma operation. To operate an MSLM in the hard-clipped thresholding mode with the negative-gamma characteristic shown in Fig. 1, the device is initially biased in the ON state at a peak on its normal $(\sin^2 \Gamma/2)$ readout characteristic. This corresponds to the point A on Fig. 2. Then, with the optical input image incident on the photocathode, V_b is ramped downwards at a pre-selected rate $\dot{V}_b$ that establishes the desired threshold exposure E_{th}. All exposures below E_{th} will be barely recorded because, at their locations, electrons cannot be removed fast enough from the crystal to prevent the gap field from eventually repelling all future primary electrons. Thus, all intensities below threshold will remain in the ON state.

Because the slope of the resulting characteristic is very steep between threshold and saturation, virtually all write light intensities above threshold are written to the maximum charge density which can be set by the terminal value of V_b to coincide with the point C (OFF state) on the device readout characteristic. Thus, operation in the nonlinear hard-clipped thresholding mode leads to the high-gamma characteristic of Fig. 1. Values of gamma in excess of 10 can be easily achieved with both the standard and Fabry-Perot devices using this technique.

Optical Feedback Configuration

Both the standard and the Fabry-Perot MSLM can be operated in the optical feedback configuration shown in Fig. 4 to realize high gamma operation. The device is first biased at the point A on its readout characteristic. As before, this is accomplished by operating the device in the open loop mode (shutter S closed), flooding the photocathode with light and adjusting the grid voltage such that the crystal charges to the uniform surface charge density σ_o. The image to be processed is then placed in the input plane P_o and transferred by lens L_o onto the crystal. The resulting modulated readout signal is then reimaged via the feedback path onto the photocathode of the MSLM. The processed output image is detected in the plane P_i.

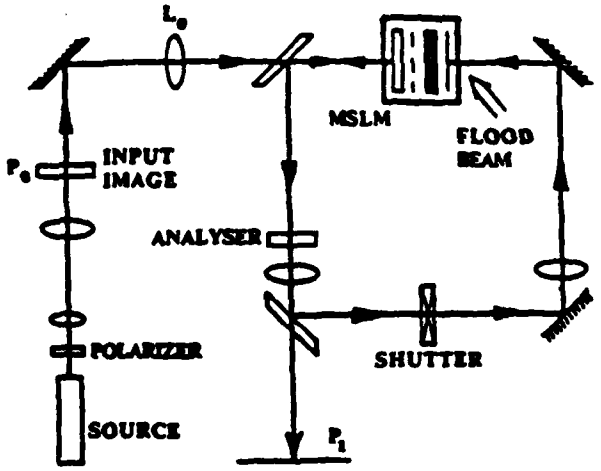

Fig. 4. Optical feedback configuration for high-gamma operation of an MSLM.

In closed-loop operation, for a given fixed uniform exposure E_o incident on the input image transparency, the high transmittance regions of the input image will at first result in strong feedback to the photocathode. This will quickly result in the deposition of a surface charge density σ_π on the crystal so as to drive the transmittance of the modulator at these points to zero (stable equilibrium). On the other hand, at the low transmittance regions of the input image, the feedback will be weak. This will result in low values of E_m that will deposit only very small amounts of additional charge on the crystal. Since these low exposures will fall below E_{th}, the transmittance of the modulator will remain high. Because the MSLM stores these charge patterns, this feedback configuration will exhibit the high-gamma characteristic shown in Fig. 1 when read out with a separate uniform source. Thus, an input image is transformed into a halftone image by this feedback configuration.

Preliminary Results

A vacuum-demountable Fabry-Perot MSLM was constructed using a 300-μm-thick $LiNbO_3$ crystal with mirror reflectivities of approximately 50% and 80% on the insulating and conducting surfaces, respectively. The insulating mirror consisted of a multiple layer dielectric coating of SiO_2 and ZrO_2. The measured readout open-loop, grid-controlled saturation characteristic of the device is illustrated in Fig 5.

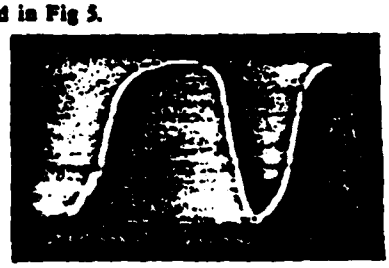

Fig. 5. Measured open loop Fabry-Perot readout characteristic of a vacuum-demountable prototype MSLM with crystal surface reflectivities of 50% and 80%.

Note the improvement over the typical sine squared characteristic of the standard MSLM. Because of the unmatched reflectivities, the contrast of the measured readout characteristic is not optimum. Nevertheless, the measured open loop gamma of this prototype Fabry-Perot MSLM is 6.2 as compared with a gamma of 2 for the standard MSLM operated in the linear mode. Closed loop gammas are expected to be much higher.

APPLICATIONS TO NONLINEAR PROCESSING

Pulse-Frequency Modulation Technique

The goal of this technique is to perform intensity to spatial frequency conversion on the input image so that subsequent Fourier-plane spatial filtering results in the desired nonlinear operation. The coding or modulation process is generally performed through the use of a contact screen. Contact screens consist of an array of cells with one- or two-dimensional spatial-frequency and transmittance variations $T_{ss}(x,y)$ within each cell.[8,9] An example of the transmittance profile of a specific one-dimensional contact screen is shown in Fig. 6.[11]

Image modulation is accomplished by sandwiching the original image and the contact screen together and imaging the combined transparency onto a high-gamma (infinite to be ideal) recording medium such as the above-described high-gamma MSLMs. The frequency of the contact screen must be sufficiently high so that within a unit cell the transmittance $T_0(x)$ of the input image transparency is constant. Thus upon readout of the high-gamma recording medium a halftone image of the original is generated.

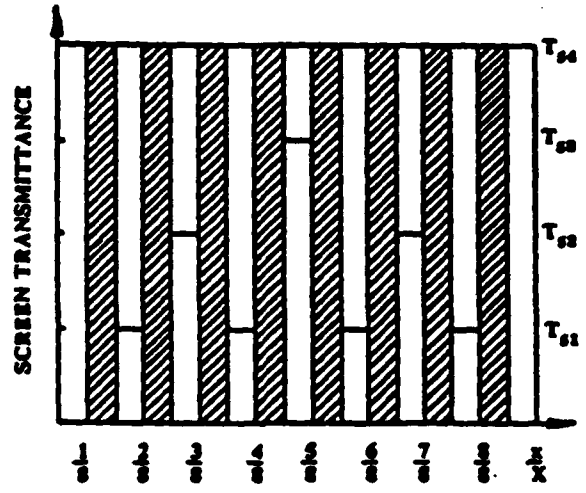

Fig. 6. Transmittance profile of the unit cell of a specific one-dimensional contact screen. Crossed-hatched regions are opaque.

The modulated halftone image is then fed into the input plane of a coherent optical processor, Fig. 7, which separates the various density levels into specific spatial frequency domains within the Fourier plane. With proper design of the screen, spatial filtering in the Fourier plane can be effectively utilized to achieve a wide range of nonlinear image and signal processing operations.

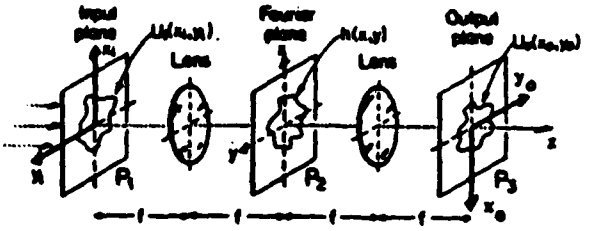

Fig. 7. Standard coherent processing system.

To further illustrate the concept of pulse-frequency modulation, consider the specific case of a one-dimensional contact screen with the unit cell transmittance pattern $T_{ss}(x)$ that is illustrated in Fig. 6. The unit cell of this screen consists of eight slits with four different transmission levels, T_{s1} - T_{s4}. Given a source of constant uniform intensity I_0, it follows that the exposure incident on the input transparency is given by $E_0 = I_0 t$, where t is the exposure time. Ignoring diffraction losses, the exposure E_m incident on the high-gamma modulator due to the typical slit within the unit cell will be given by

$$E_{ma} = E_0 T_0 T_{sa}; \quad a = 1, 2, 3, 4, \tag{6}$$

where a is a label denoting slits of the same transmittance, and T_0, the local transmittance of the input image transparency, is assumed to be constant over the unit cell. Note that for the given screen $E_{ma} > E_{m(a-1)}$.

Because the modulator exhibits the threshold characteristic illustrated in Fig. 1, the spatial frequency modulation of its readout light will be dependent on the exposure E_{ma}. For example, given a fixed exposure E_0 incident on the input transparency, if within a given cell T_0 is such that $E_{m4} < E_{th}$, then all E_{ma} for that cell will be below threshold, and the cell will have a uniform transmittance of nearly unity. Thus the modulator readout light from that cell will be spatially unmodulated. That is, its grating carrier spatial frequency would be zero ($f_{gx} = 0$). Likewise, if T_0 is such that $E_{m4} \geq E_{th} > E_{m3}$, then the modulator readout light from that cell will be modulated by a grating with spatial frequency $f_{gx} = 1/X$. For $E_{m3} \geq E_{th} > E_{m2}$, $f_{gx} = 2/X$, _ and for $E_{m1} \geq E_{th}$, $f_{gx} = 8/X$.

When this pulse-frequency modulated image is injected into the conventional coherent optical processor, the diffraction spot at spatial frequency coordinate $f_x = f\lambda/X$ in the Fourier plane will contain the information corresponding to points in the input image with T_0 governed by $T_{s4} T_0 \geq I_{th}/I_0 > T_{s3} T_0$. Here f is the focal length of the Fourier transform lens, λ is the wavelength of the readout source and I_{th} and I_0 are the intensities corresponding to E_{th} and E_0, respectively. Similarly, the spot at $f_x = f\lambda 2/X$ contains the image information corresponding to $T_{s3} T_0 \geq I_{th}/I_0 > T_{s2} T_0$, etc.

Several experiments can then be performed. For example, by measuring the intensities of the spots in the Fourier plane, a histogram of the original image can be obtained. Second, if different neutral density filters that have higher densities for the spectra with lower intensities are placed behind these spots and all other diffraction orders are stopped, the output image contrast will be enhanced. Third, if a white light readout source is used instead of a monchromatic source, and a set of color

filters are placed at the Fourier plane to selectively pass certain colors, a pseudo-color image will be obtained. Finally, if a set of optical wedges with different wedge angles are placed behind the Fourier plane diffraction spots, artificial stereo pictures will be obtained. These are just a few of the nonlinear processing operations that can be realized with this technique. These experiments are now in progress. Future results will be published elsewhere.

ACKNOWLEDGEMENTS

This research was sponsored in part by the Physics Division of the U.S. Army and the National Aeronautics and Space Administration. The authors would like to thank D. Z. Zhao for helpful discussions.

REFERENCES

1. P. F. Muller, "Linear Multiple Image Storage," Appl. Opt. 8, 267 (1969).
2. F. T. S. Yu and M. S. Dymek, "Optical Information Parallel Processing: a Technique," Appl. Opt. 20, 1450 (1981).
3. D. Z. Zhao, C. K. Chiang, and H. K. Liu, "Quantitative Optical Image Subtraction by Means of Pulse-width Modulation Through One-dimensional Contact Screens," Optics Lett. 6, 490 (1981). Also, "Contact Screen Image Subtraction Technique," Appl. Opt. 20, 4234 (1981).
4. H. Kato and J. W. Goodman, "Nonlinear Filtering in Coherent Optical Systems Through Halftone Screen Processes," Appl. Opt. 14, 1813 (1975).
5. S. R. Dashiell and A. A. Sawchuk, "Nonlinear Optical Processing: Analysis and Synthesis," Appl. Opt. 16, 1009 (1977).
6. M. A. Karim and H. K. Liu, "All Optical Homomorphic Image-Processing System," 7, 371 (1982).
7. S. R. Dashiell an A. A. Sawchuk, "Optical Synthesis of Nonlinear Nonmonotonic Functions," Opt. Comm. 15, 66 (1975).
8. T. C. Strand, "Nonmonotonic Nonlinear Image Processing Using Halftone Techniques," Opt. Comm. 15, 2394 (1976).
9. H. K. Liu, J. W. Goodman, and J. Chan, "Equi-densitometry by Coherent Optical Filtering," Appl. Opt. 15, 2394 (1976).
10. S. R. Dashiell and A. A. Sawchuk, "Nonlinear Optical Processing: Nonmonotonic Halftone Cells and Phase Halftones," Appl. Opt. 16, 1936 (1977)
11. H. K. Liu and J. W. Goodman, "A New Coherent Optical Pseudo-Color Encoder," Nouv. Rev. Optique, 7, 285 (1976).
12. H. K. Liu, "Coherent Optical Analog-to-Digital Conversion Using a Single Halftone Photograph," Appl. Opt. 17, 2181 (1978).
13. F. T. S. Yu and A. Tai, "Incoherent Image Addition and Subtraction: A Technique," Appl. Opt. 18, 2705 (1979).
14. W. Schneider, "Spatial Pulse Modulation for Coherent Optical Densitometry," Opt. Acta. 21, 263 (1974).
15. G. Indebetouw, "Production of Color Coded Equidensities Using Non-linear Filtering," Appl. Opt. 16, 1951 (1977). Also, "New Method of Pseudo-Color Equidensitometry," Appl. Opt. 18, 4206 (1979).
16. B. H. Soffer, et al, "Variable Grating Mode Liquid Crystal Device for Optical Processing," SPIE 218, 81 (1980).
17. C. Warde, A. M. Weiss, A. D. Fisher and J. I. Thackara, "Optical Information Processing Characteristics of the Microchannel Spatial Light Modulator," Applied Optics 20, 2066-2074, (1981).
18. C. Warde, and J. I. Thackara, "Oblique-cut $LiNbO_3$ Microchannel Spatial Modulator," Opt. Lett. 7, 344-346, (1982).
19. C. Warde, and J. I. Thackara, "Operating Modes of the Microchannel Spatial Light Modulator," Opt. Eng. 22, 695-702 (1983).
20. R. Dillon and C. Warde, "X-ray Imaging Characteristics of the Vacuum-Demountable Microchannel Spatial Light Modulator," Opt. Eng. 24, 269-273 (1986).
21. T. Hara, Y. Ooi, T. Kato and Y. Suzuki, "Microchannel Spatial Light Modulator with Improved Resolution and Contrast Ratio, PROC. SPIE, 613-25, 1986.
22. Ch. Thum., "Histograms of Continuous Tone Image by Transformation and Integration," Angewandte Optik, Annual Report, 31 (1980).
23. K. A. Stetson, Optik 29, 386 (1969).
24. A. A. Sawchuk, "Artficial Stereo," Appl. Opt. 17, 3869 (1978).
25. H. K. Liu, "Halftone Screen with Cell Matrix," U.S. Patent No. 4188225, Feb., (1980).

A reprint from O-E LASE '86
Conference on Optoelectronics and Laser Applications
Nonlinear Optic, January 19-24, Los Angeles, CA

An optical inner-product array processor for associative retrieval

S. Y. Kung

Department of Electrical Engineering, University of Southern California
Los Angeles, CA 90089-0272

and

H. K. Liu

Jet Propulsion Laboratory, California Institute of Technology
Pasadena, CA 91109

Abstract

In this paper, an inner-product array processor for the associative retrieval problem is presented. First, the algorithm and architecture of the array processor design are discussed. Then an optical implementation scheme is proposed. The matrix model of the associative memory is adopted. In this model, if one of the M vectors is to be reliably recalled, the dimension of the vectors, N, must be much larger than M. By taking advantage of this fact, our result offers a factor of $\sqrt{N/M}$ saving on the matrix elements. More significantly, real-time inputting and updating of the matrix elements can be potentially implemented with existing space-variant holographic elements and recently discovered liquid crystal television spatial light modulators.

I. Introduction

Optical array processors have a great potential because of their parallelism, high computational rates, small size and weight, and their low power dissipation and cost. These processors naturally offer the same strength of VLSI in terms of massive parallelism and yet circumvent the limitation on communication inherent in VLSI processors.

In this paper, we discuss an optical processor design for an associative retrieval processing system. We shall first present a brief history of the evolution of distributed associative memory networks, and the essential algorithmic and architectural design considerations. These then lead to a unique optical implementation of the inner-product array processor for the associative-retrieval problems. There are two memory types in the current computer design; one is location addressable and the other is content addressable. It has been recognized that the content-addressable type is more closely related to how the human brain functions. In fact, a popular approach to its implementation is based on one which resembles that of a neuro-network. Neural signals are trains of pulses with variable frequencies. The task of memory is to reproduce the neural signal at the places where they earlier occurred. This leads to the notion of associative memory network and associative retrieval, whose main features include recognition and error correction based on partial or cluttered input.

II. A Brief Historical Note

Since the 1970's, the correlation matrix model of the distributed associated memory network has been gaining popularity. Notably, Kohonen, Nakano, and Anderson have done independent work in this area in the early 1970's. A brief history is presented below, and key references are provided for researchers who have interests in more details of the evolution of associative memory networks.

Note that the conception of associative memory can trace all the way back to Aristotle's work [370 B.C.] on memory and reminiscence. The cybernetic research work in 1950's on learning digital neworks, perceptron, and conditioned connection crossbars [1-3] has paved ways for the modern era of studies on the subject. In the 1970's, the matrix model (as distinguished from the connection model) of memory networks seems to have gained the attentions of many researchers. These work are represented by Morishita [4], Kohonen [5], Nakano [6], Anderson [7]. More recently, Hopfield [8] further extended the previous works to structure a computational model by a notion of energy functions with an outer-product computing model on a iterative basis. To memorize a number of, say M, N-tuple vectors, Hopfield has found through computer simulations that a vector among M can be successfully recalled if M is less than 0.15N.

III. An inner-product computing model for associative retrieval

One of the most elementary operations implemented by associative memory is the associative recall system. While Psaltis and Farah [9, 10] have presented the optical implementation of associative recall model based on the outer-product of the matrix, we propose a model that is based on the inner product of the matrix with an array of M matrices. The dimensions of each matrix in the array are $\sqrt{N} \times \sqrt{N}$ and the array is $\sqrt{M} \times \sqrt{M}$. We assume that $\sqrt{N}$ and $\sqrt{M}$ are integers. The dimensions of the array are $\sqrt{M}\sqrt{N} \times \sqrt{M}\sqrt{N} = MN$ which is less than the dimensions N x N of the outer-product matrix model since N > M.

Referring to Figure 1, the iterative computation is represented by

$$V^* \leftarrow\!-\!-\!- T_\theta\,[AV] \tag{1}$$

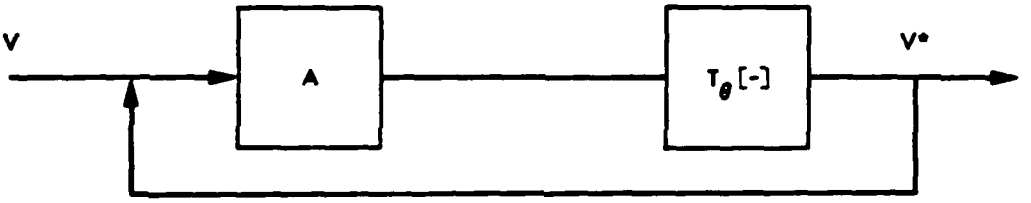

Figure 1. An iterative computing model for associative retrieval.

where A is a N x N associative-recalling matrix, which is assumed to be "pre-taught" (i.e., non-adaptive), and $T_\theta[\cdot]$ is a thresholding operation with threshold = θ. In the non-adaptive case, the rank of A is always equal to the total number of information patterns, M. If the columns of A, representing memorized patterns, are nearly orthogonal, then a pattern may be retrieved by its partial information. In order to guarantee a robust and reliable information retrieval, M should be much smaller than the total number of features, N, for example M < 0.15 x N. This implies that A can be expressed as

$$A = \sum_{i=1}^{M} V_i\, U_i^T,$$

for a set of vectors $\{U_i, V_i\}$; i = 1,...,M. (Under the special circumstance of "auto-associative" recall, then $U_i = V_i$.)

The inner product array processor exploits the fact that M<<N, and achieves a considerable amount of hardware savings. The computation in Eq. (1) now becomes

$$A\gamma = \sum_{i=1}^{M} V_i\, U_i^T \gamma, \tag{2}$$

This can be subsequently decomposed into four steps:

Step (1) $X_i = U_i^T V$, for i = 1 ..., M;

Step (2) $Y_i = V_i X_i$ for i = 1,... M;

Step (3) $Z = \sum_{i=1}^{M} Y_i$;

Step (4) $V^* = T_\theta\,[Z]$;

The four separate steps of this new computing model are depicted in Figure 2.

Referring to the schematic diagram in Figure 2, both the I.P.O. and V.S.O. may be implemented in parallel via an optical array processor. In this case, each N-dimensional I.P.O. (or V.S.O.) may be implemented by one $\sqrt{N} \times \sqrt{N}$ "optical-plane-product," as shown in Figure 3. This means that a much more compact-size optical implementation process is now possible.

IV. A optical implementation of a programmable associative recall system

An optical system for implementing the inner-product associative-retrieval model as

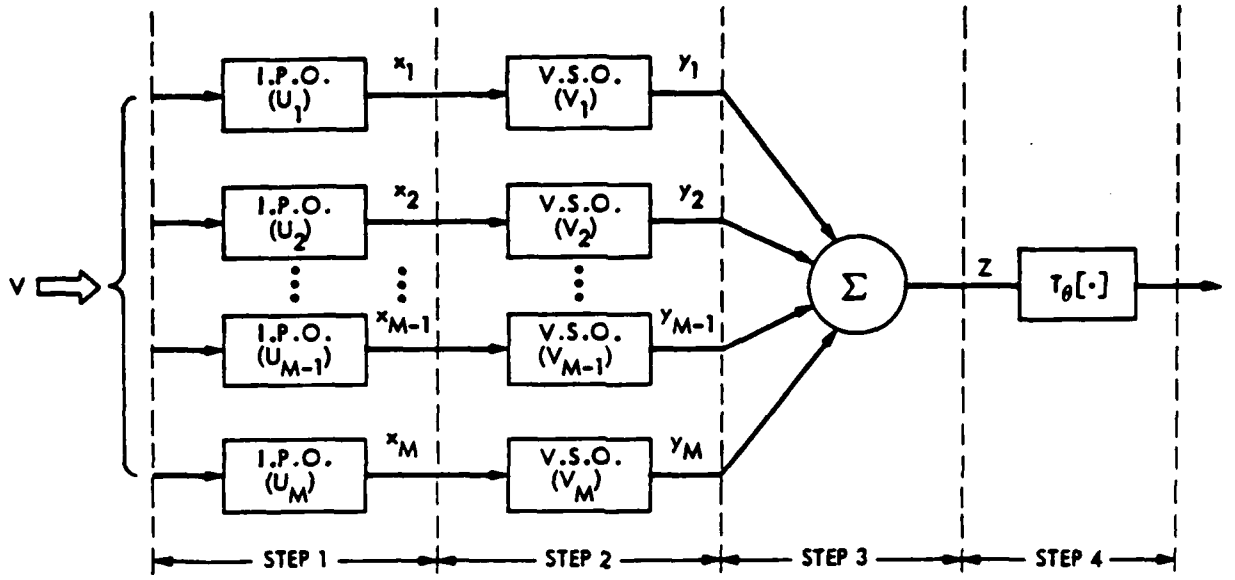

Figure 2. The inner product computing model where I.P.O. represents an inner product operator and V.S.O. represents a vector scaling operation.

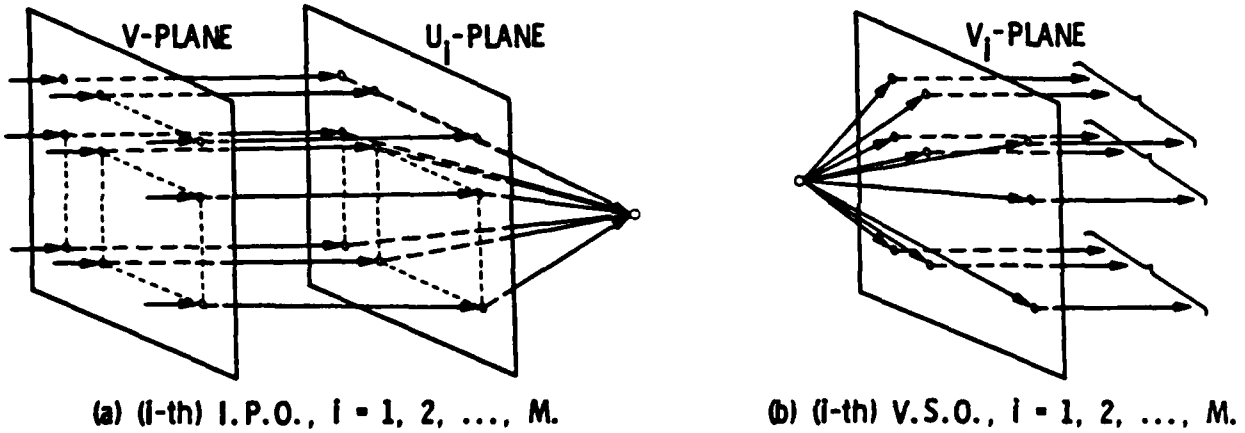

Figure 3. A schematic diagram of the optical implementation of I.P.O. and V.S.O.

discussed above is shown in Figure 4. In the Figure, a liquid crystal television (LCTV) is used as an electronically addressed spatial light modulator (SLM). In fact, other electronically addressable SLM's such as the Hughes CCD-addressed LCLV may also be able to serve the same function as the LCTV. Two multiple-focus holographic lenses[12] (hololens), MHL1 and MHL2 are used as space-varient optical elements for performing the necessary inner-product and summation functions. The function or capability of the MHL's is shown in Figure 5. The holographically-made optical element is capable of replicating an input 2-D image by first focusing it to an array of focal points at its focal plane and then forming an array of images at its image plane. All the replicated images are derived from a single image through the common aperture of the MHL; a capability that cannot be achieved by any currently available refractive elements such as a glass lens.

To set up the optical array processing system, we first display the M known vectors on the LCTV each in a $\sqrt{N}$ by $\sqrt{N}$ matrix format. The nature of the LCTV's transmissive screen is to modulate the input laser light by what is being written according to the matrix-format vector. The $\sqrt{M}$ x $\sqrt{M}$ matrices being written or displayed on the LCTV screen exhibit its storage capacity and the transmission modulation property of the screen enable these matrices to be multiplied by other matrices. Hence once the writing process is completed, the storage step is done.

To activate the addressing-recalling mode of operation of the system, an input vector can be invoked. The N-tuple vector should be of the same matrix format as that of any one

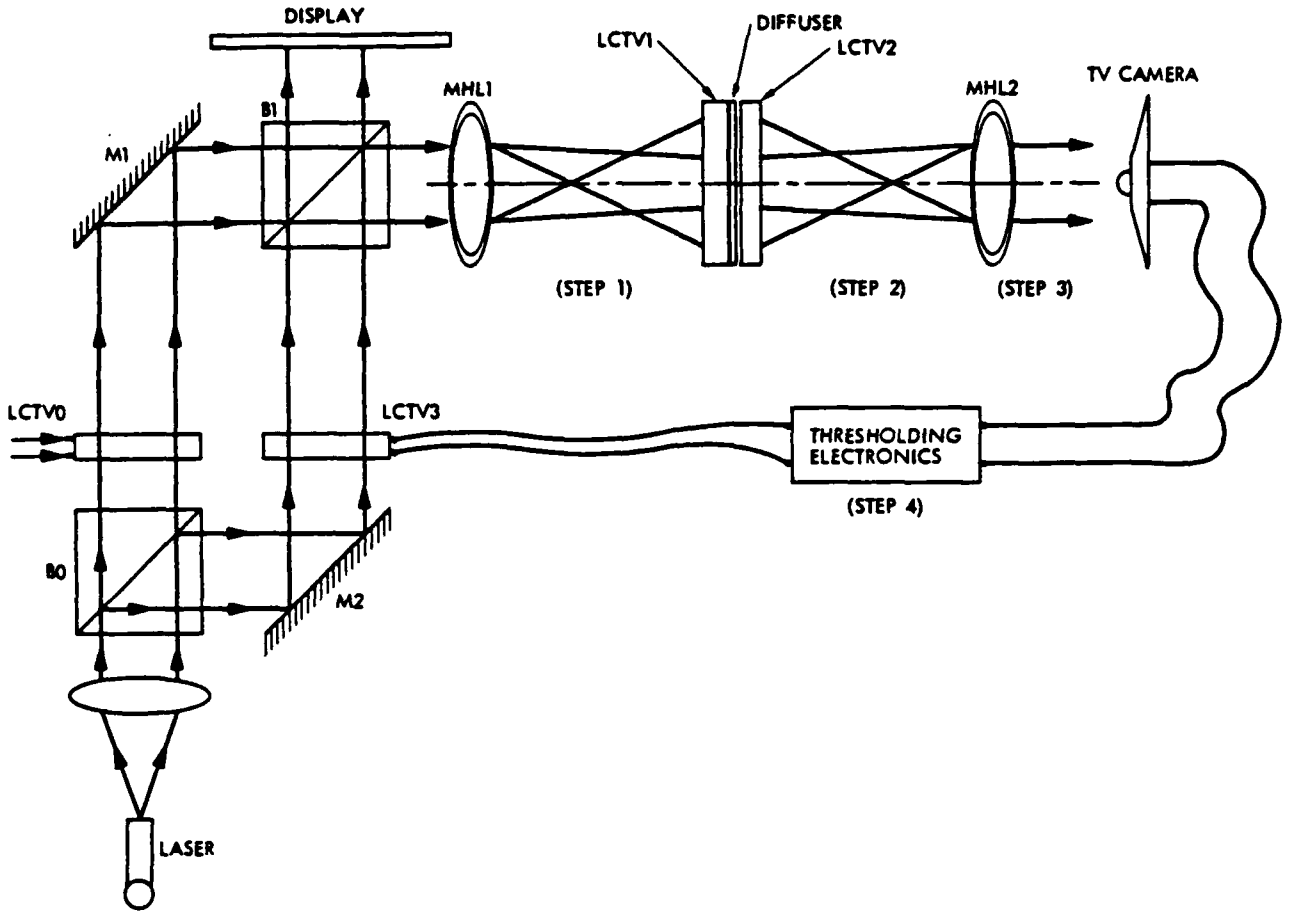

Figure 4. A schematic diagram of an optical implementation of the inner-product array processor.

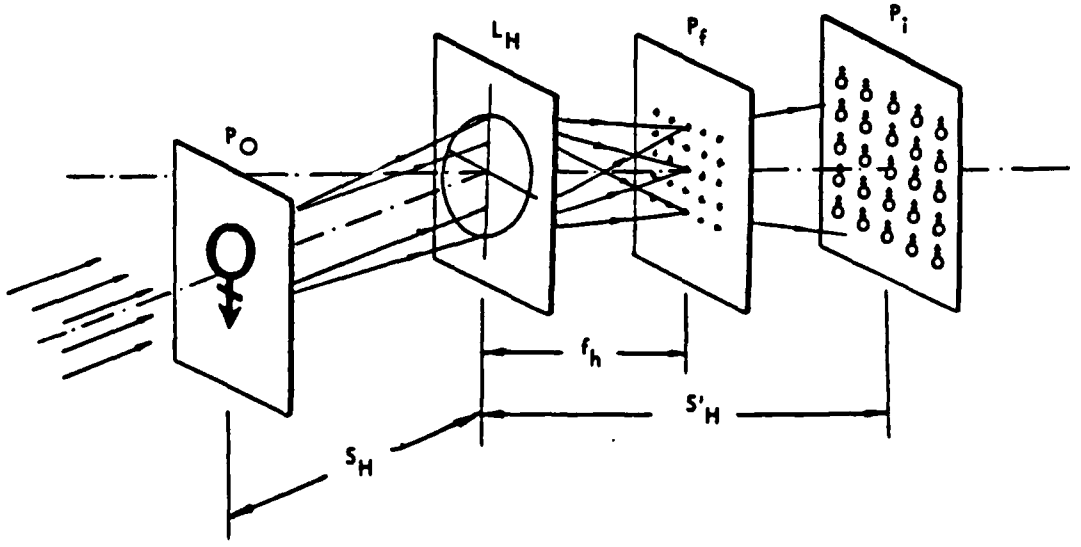

Figure 5. The function of a multiple-focus holographic lens.

can be invoked. The N-tuple vector should be of the same matrix format as that of any one of the M vectors so that it can be written onto LCTVO. The screen of LCTVO can then be used to modulate the collimated laser beam through the cube beam splitter BO. The information being written on LCTVO can then be sent to address the M vectors. After the

light carrying the vector information transmitted through B1 and MHL1, it is replicated to a $\sqrt{M}$ by $\sqrt{M}$ (here we assume that $\sqrt{M}$ is an integer) array of matrices of $\sqrt{N}$ x $\sqrt{N}$ dimensions of elements coinciding matrix by matrix with what has been previously stored in LCTV1. The inner-product-type operation is thus partially achieved at this step. To complete the entire inner product process, the multiplied results are followed by a diffuser which averages the light intensity and yield the M inner-product scalars. The scalars are then transmitted through to another array of M known vectors displayed (or written) on LCTV2. (Computationally, this process implies that the M vectors are multiplied with the scalar.) The matrix array on LCTV1 and LCTV2 should be identical in case of auto-associative retrieval. Finally, the weighted vectors (or matrices) are summed up by MHL2 which plays a reversed role as MHL1. A TV camera or CCD detector array can be used to detect the output. The output should be thresholded by an electronic device. (The thresholded array may also be performed by an optical device if a high-gamma spatial light modulator is available.) If the electronic device is adopted (as shown in Figure 4), the thresholded result can be written on LCTV3 and illuminated by a collimated laser light from BO. This thresholded matrix is then used as a feed-back input through B1 and MHL1 ready for a new iteration process.

The above-mentioned procedure will repeat until a steady-state is reached and exhibited in the display sent also through B1. Once the steady-state is reached, the retrieval process is thus completed.

A partial optical set-up of the inner-product associative-retrieval model is shown in Figure 6. In the forefront, a LCTV imbedded in a liquid gate is shown. The electric connection to the LCTV is also visible. At this stage, the set-up is only for the purpose of testing the quality of the LCTV in its applications as a spatial light modulator. The results of the testing are important to the implementation of the associative-retrieval model.

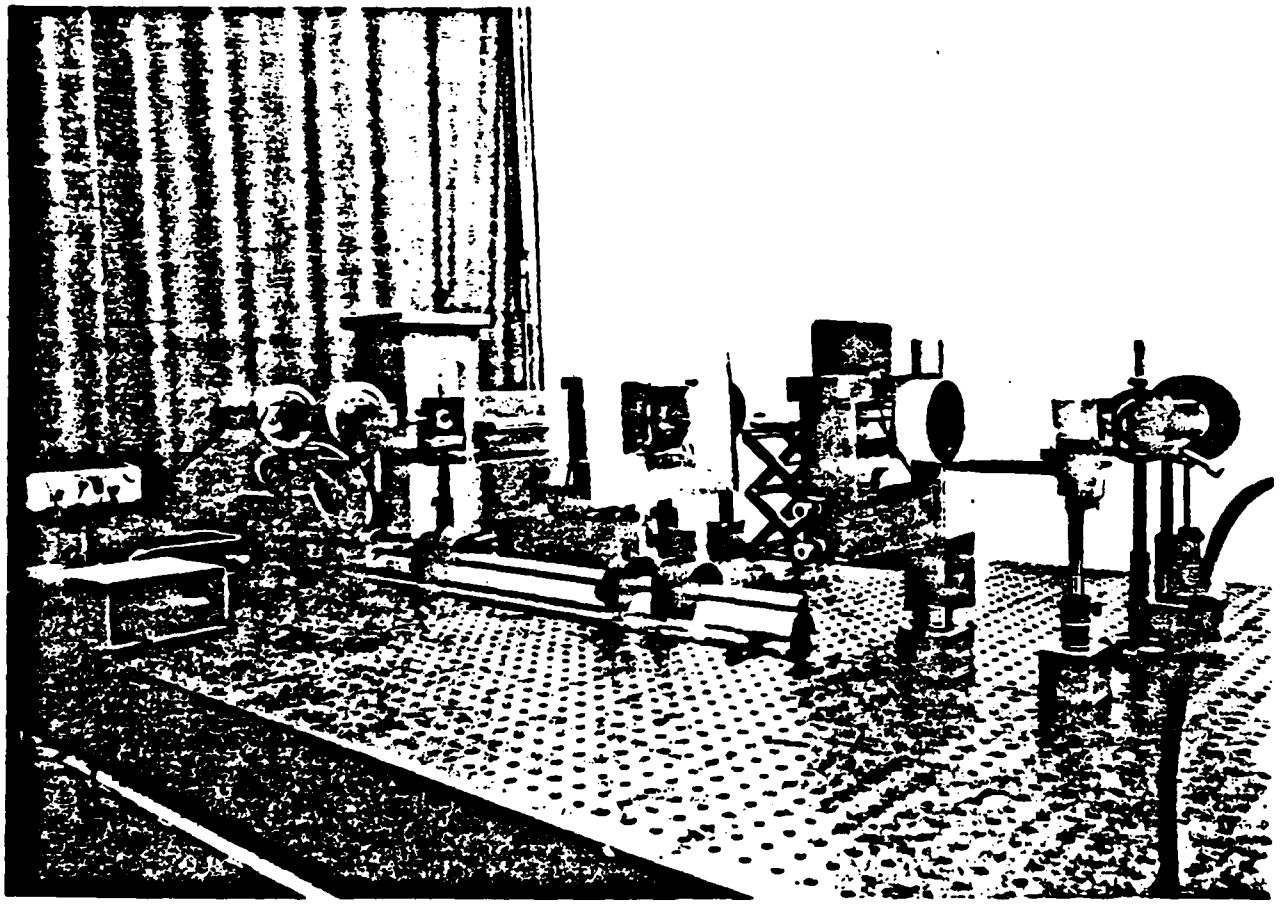

Figure 6. A photograph of a part of the laboratory set-up of the optical inner-product array processor.

V. Conclusions

The principle and implementation of a programmable associative recall system based on the inner-product model have been described. Advantages of the system include:

1. The dimensions of the matrix in the computation have been reduced. For example, in the Kohonen-Nakano-Hopfield model, the dimension of the required memory matrix is N x N. Whereas in the present case we only need an array of M matrices of dimension $\sqrt{N}$ x $\sqrt{N}$. Numerically, if N = 100 and M = 4, then a 2 x 2 array of 10 x 10 matrices is required in the inner-product model, instead of a 100 x 100 memory matrix. If N = 900, M = 100, then a 10 x 10 array of 30 x 30 matrices is sufficient to perform the retrieval function. Therefore, one order of magnitude of saving on the memory matrix elements can be achieved and make the optical implementation more feasible.

2. The optical implementation exploits the newly developed inexpensive LCLV as spatial light modulators and multifocus lens as the replicating, holographic interconnecting, and matrix-matrix multiplication processors.

3. Real-time modification of the memory can be achieved by changing the matrix elements through electronically reprogramming the LCTVs.

We are hopeful that the proposed inner-product model, once realized, will be very useful for many associative memory applications.

Acknowledgment

This research was supported in part by NASA, Army Research Office, National Science Foundation Grant ECS-82-13358, and Office of Naval Research Contract No. N000014-85-K-0599.

References

1. B. G. Farley and W. A. Clark, "Simulation of Self-Organization Systems by Digital Computer", IRE Trans. IT-4, 76, (1954).

2. F. Rosenblatt, "The Perception: A probablistic model for information storage and organization in the brain", *Psych. Rev.* 65, 386, (1958).

3. K. Steinbuch, "The learning matrix", Kybernetik, 1, 36, (1961).

4. I. Monishita, "Analysis of an adaptive threshold logic unit", IEEE Trans. C-19, 1181 (1970).

5. T. Kohonen, "Correlation matrix memories", Helsinki U of Tech. Report TKK-F-A/30, i.b.i.d. IEEE Trans. C-21, 353 (1972).

6. K. Nakano, "Associatron-A model of associative memory" IEEE Trans. SMC-2, 380, (1972).

7. J. A. Anderson, J. W. Silverstein, S. A. Ritz and R. S. Jones, "Distinctive features, categorical perception, and probability learning: some application of a neural model", Psych. Rev. 84, 413, (1977).

8. J. J. Hopfield, "Neural network and physical systems with emergent collective computational abilities:, Proc. Natl. Acad. Sci. USA 79, 2554, (1982).

9. D. Psaltis and N. Farhat, JCO-13, August, 1984, Saporo, Japan.

10. D. Psaltis and N. Farhat, Optics Letters, 10, 98, (1985).

11. H. K. Liu, J. A. Davis, and R. A. Lilly, Optics Letters, 10, 635 (1985).

12. Y. Z. Liang, D. Zhao, and H. K. Liu, Appl. Opt. 22, 3451, (1983).

END

11-86

DTIC